INTERNATIONAL JOURNAL OF SYSTEMS APPLICATIONS, ENGINEERING & DEVELOPMENT
Issue 2, Volume 2, 2008

Study of contact resistance for high copper alloys under indentation and insertion forces

R. El Abdi and N. Benjemaa

Abstract**—**The purpose of this paper is to present an experimental and a numerical study of simple geometries representing the electrical contact in automotive connectors (a sphere-plane and cylinder–plane electrical contact) when a current passes through them. High copper alloys were used to improve mechanical and electrical connector behaviour.
Changes in the electrical contact resistance versus force in the range of 1-100N for different sizes and geometries were studied. The designed samples were subjected to indentation (static contact) and insertion (sliding contact). The temperature evolution for different copper alloys was studied for different forces and currents. The temperature reached near the contact area, between two solids constituting the contact, is a significant parameter to indicate the damage level. However, it is very difficult to know the inner temperatures. A finite element simulation code including the roughness contact surface profile was carried out in order to obtain the internal temperatures. Experimental power law of contact resistance versus forces was obtained where the law parameters are well related to electrical resistivity, Young modulus, yield stress.
On the other hand, a numerical size optimization was carried out to obtain the resistance gain or the volume gain with mechanical, geometrical and physical constraints.

Key-words**—**Electrical contact resistance, temperature, finite element method, optimization, contact zone.

I. INTRODUCTION

THE increase in electronic controls in transport, machining and numerous other industrial and domestic applications has induced a fantastic increase in connector applications during the last decades. The connectors for automotive applications are often subjected to harsh environmental conditions. Long term exposure to extreme levels and rapid variation, humidity and temperature deteriorate the connectors and reduce reliability [1]. However, the ability of the connectors to withstand high temperatures has become critical since the engine compartment which experiences ambient temperatures has slowly decreased in size because of the more compact and low hood line design.

R. El Abdi is with the Rennes1 University (Applied Mechanical Laboratory LARMAUR). IUT de Rennes. 3, Rue du Clos Courtel. B. P. 90422- 35704 Rennes cedex 7 FRANCE (corresponding author to provide phone: 33 2 23 23 41 12; fax:33 2 23 23 41 12; e-mail: relabdi@univ-rennes1.fr).

N. Benjemaa is with Rennes1 University, Rennes Institut of Physics (Equipe Contacts Electriques). Université de Rennes1. Campus de Beaulieu. Bât. 11B. Avenue du Général Leclerc. CS 74205. 35042 Rennes Cedex. FRANCE

Though it is very difficult to simulate the exact conditions of the automobile connectors encounter in real life, it is possible to study the effect of certain conditions and to correlate their influence on the extent of temperature variation and in turn to predict the reliability of connectors. Much work [2-9] has been devoted to understanding the contact zone mechanisms but their complexity led us to study a simple contact shape with former copper alloys.

No study to date, has studied the influence of roughness on the changes of resistance in the contact zone for high copper alloys. In this work, different sizes and geometries (sphere-plane and cylinder–plane electrical contacts) were analyzed. Samples were subjected to different contact loads and different current values in the indentation tests. When the roughness profile is taken into account, the finite element model [10-11] leads to an improvement of the numerical resistance values. The temperature near the contact zone was measured for different currents and indentation forces. It was shown that material resistivity has a non negligible influence on temperature evolution. Finally, a numerical design optimization was undertaken to obtain optimum contact resistance with several mechanical, electrical and physical constraints. To minimize the connector mass, another design optimization was carried out when the objective function was the sample volume.

II. HIGH COPPER ALLOYS USED AND EXPERIMENTAL SET-UP

A. Materials used

The present study analyses the contact resistance evolution for high copper alloy samples (Table 1).

Table 1 Characteristics for different copper alloys used

Copper alloy	Composition	Yield stress (MPa)	Thermal conductivity (W/mK)	Electrical resistivity (Ω.mm)
C12200 (A)	Cu 99.9%+ 0.002% P	200	340	$2.12\ 10^{-5}$
C10100 (B)	Cu 99.99	200	401	1.6810^{-5}
C70250 (C)	$CuNi_3SiMg$	514	190	$4\ 10^{-5}$
C19400 (D)	$CuFe_2P$	401	280	$2.7\ 10^{-5}$
C18070 (E)	CuCrSiTi	420	310	$2.2\ 10^{-5}$
C19210 (F)	CuFeP	322	350	$1.88\ 10^{-5}$
C14415 (G)	CuSn0.15	333.5	350	$1.96\ 10^{-5}$

The samples with a U shape (Fig. 1) were made with a sheet of 20 mm width, using the processing technique of stamping and bending. The two parts of the sample (plane part or lower part and a sphere (or cylinder) part (or upper part) have the same thickness i.e. 0.8 mm. The radius of the sphere segment (or cylinder segment) was 3 mm (Fig. 1).

 Manuscript received April 24, 2008; Revised June 12, 2008

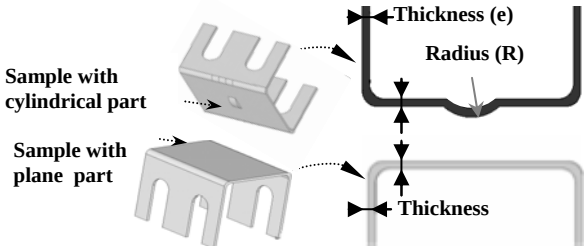

Fig. 1 U-shaped samples

Before each test, the sample surfaces were cleaned by an antioxidant paste and then dipped into an ultrasonic alcohol bath. Three new samples were used in each test.

The experimental measurement bench was monitored by a microcomputer over a GPIB bus and instrument. This enables a low stepping motor to be used for progressive force loading and current sourcing, contact voltage measurement and data collecting. The first following test was carried out to simulate indentation phase. This test consisted in applying a progressive contact vertical force Fc: (2, 4, 8, 16, 32, 64 and 100 N) (Fig. 2a) for measuring the contact resistance. The second test consisted in applying normal forces at the same upper values then enables a sliding of 1mm by F_i force to simulate the insertion. The contact resistance was measured at the end of each insertion step (Fig. 2b).

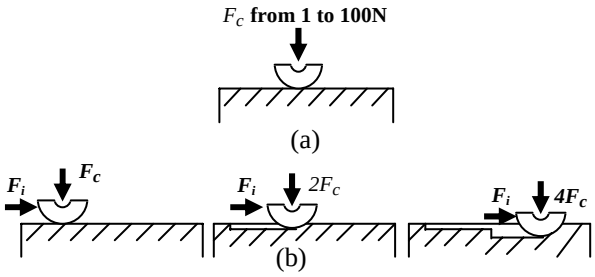

Fig. 2 Sample under (a) indentation load (spherical /plane contact) and (b) under insertion test

B. Experimental set-up

The resistance or temperature measurements were started at different desired times. Since the geometry of the flat and reader specimen were relatively small, thermo-couples with high response times (J type) were used. Figure 3 details the electrical circuit used. An electrical current of 10 A was applied to an electrical circuit. A microvoltmeter (Keithley) with 1 µV resolution, was used to measure the fall of potential by the ‘‘four wire’’ method. Thus, the contact resistance during indentation phase could be obtained.

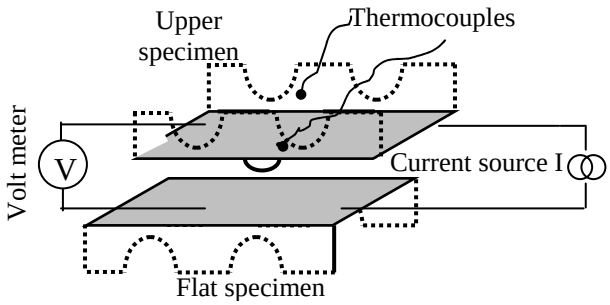

Fig. 3 Geometry of the rider and flat samples and the circuit used to measure the contact resistance

III. FINITE ELEMENT MODELLING

Simultaneously with the experimental tests, a numerical modelling is undertaken. One can suppose that the contact surface is smooth (without roughness) or one can take into account the real roughness profile in the numerical modelisation. Two finite element models are proposed with or without the contact surface roughness. The measurement of the roughness profile was obtained with the help of a profile meter. Regarding the symmetric form of the sample parts, only half of the samples were meshed. Figures 4a and 4b give the adopted meshes and the zoom of the contact zone for a cylindrical contact, when the roughness profile is introduced in the numerical modelling.

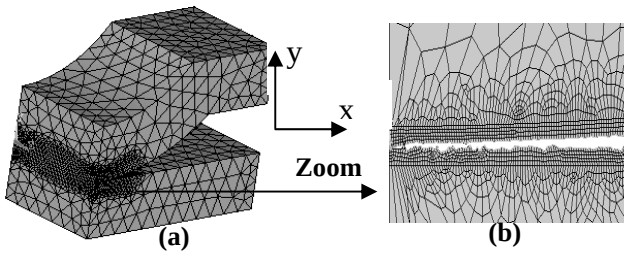

Fig. 4 Finite element meshes and zoom of the contact zone with roughness profile (cylindrical /plane contact)

Simulation of the displacement for a symmetric model and the large deformations with elasto-plastic behaviour was obtained with the Ansys finite element (Ansys [10]) code. Underlying the approach in this code is the discretization of the continuum involved. Also, an important feature of this program involved the ability to model the contact between the spherical part and the plane part as a sliding interface. As the spherical part goes down during the indentation test, the software detects the nodes in contact to evaluate the contact surface. For the mechanical calculus, axisymmetric element types were used: axisymmetric structural solid node element (Plane183) and 3 nodes surface to surface element for the contact area (Conta172) and target area (Targe169). For the electrical calculus, eight plane nodes coupled with field solid elements were used (Plane 223- 2D). The contact algorithm used is the Augmented Lagrangian method.

Contact, material and geometric non-linearities required a full Newton Raphson scheme to be used with the sparse matrix solver (direct solver).

The program checked the convergence of the iterative solution by using a force criterion. The friction coefficient μ between two surfaces in contact (copper alloy/copper alloy) was equal to 0.2. It is essential to note that in this study the indirect coupling solution was used. The program was used with 9 817 elements and 28 313 nodes for the axisymmetric model with the roughness modelling. A total of at least 708 elements were allowed to come into contact with the plane part in order to provide sufficient resolution in the computation of the field around the spherical part. Other smoothness meshes were tested. The conclusion was that the results were identical. To get better results, the contact zone was refined (Fig. 4, Zoom of the contact zone).

Due to the axisymmetric configuration, the boundary conditions may be expressed as follows:

$$Uy\ (y = -0.8) = 0 \quad (1)$$

where y = -0.8 (mm) denotes the lower surface of the plane part,

$$Ux\ (x = 0) = 0 \quad (2)$$

where x = 0 denotes the axisymmetric conditions. Uy, Ux are respectively the displacement according to y and x axis (Fig. 4).

IV. Current and Force Influences.

The C19210 (F) alloy presents a low resistance in comparison with the other copper alloys used. Fig. 5 gives temperature changes concerning this copper alloy for cylindrical contact for one indentation test. Note that the temperature (noted ΔT) is the difference between the ambient laboratory air temperature (equal to 22°C) and the real temperature near the contact zone. The temperature increases with time and the current is the dominating parameter which influences the increasing temperature values. Lower loads lead to a small contact surface and thus to small temperature values.

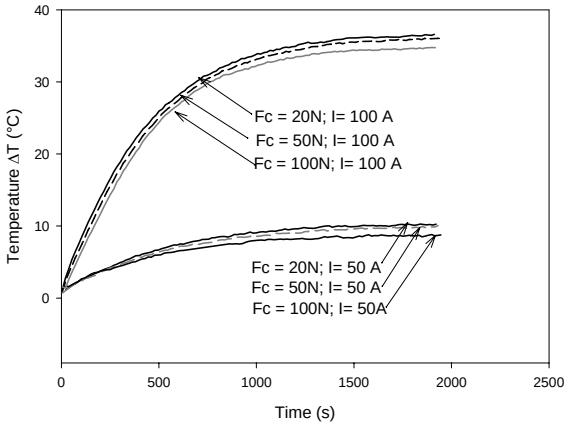

Fig. 5 Temperature evolution for C19210 (F) copper for cylindrical contact

On the other hand, electrical contact resistance decreases inversely to the applied load (Fig. 6). When the roughness profile is taken into account, numerical modelling leads to a good approximation to the experimental results (Fig. 6: numerical results for cylinder (with roughness)).

The same conclusions were obtained for the other high copper alloys. For the same conditions, one can note that the experimental results, when a spherical contact is used, leads to lower electrical contact resistance values (Fig. 6). The sphere/plane contact led to lower contact resistance values, which are thus more interesting for the connector manufacturers whose first concern is to minimize this resistance.

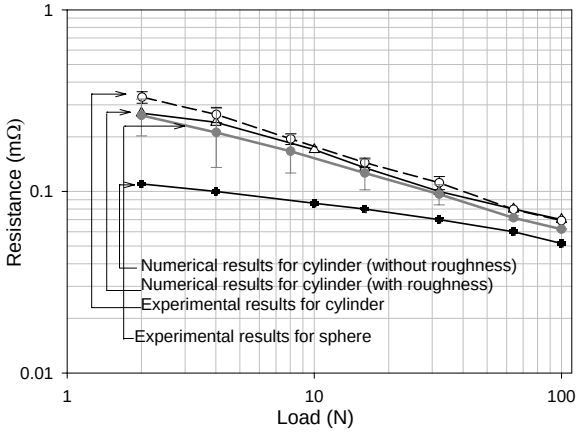

Fig. 6 Contact resistance for cylindrical and spherical contact for C19210 (F) copper alloy

Fig. 7 gives the temperature evolution for different applied loads and different current values for different copper alloys for a spherical contact. The copper alloys are classified according to ascending electrical resistivity value (C10100 (B) has the lowest resistivity and C70250 (C) has the highest resistivity – Table 1). Temperature increases according to the electrical resistivity of the studied material. High current leads to high temperatures for whatever the applied force. The high contact forces lead to large contact zones and thus to a lower temperature.

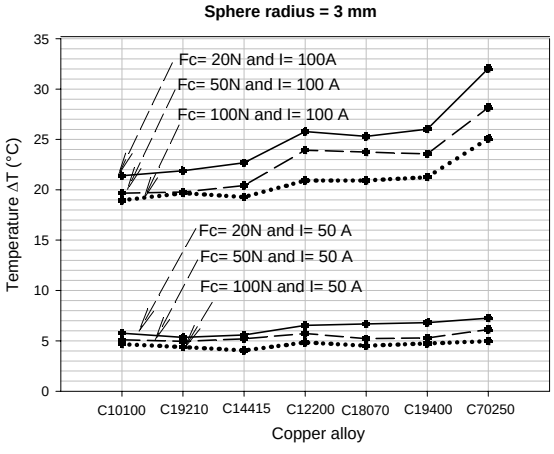

Fig. 7 Temperature evolution for different copper alloys under spherical contact

V. Power Law of Contact Resistance

A. Indentation test

For all materials listed in Table 1 and submitted to indentation test, experimental contact resistances R_c

versus contact forces F_c are given in Fig 8. In this double logarithmic scale, the contact resistance decreases linearly with forces and can be fitted to a power law: $R_C = K_C F_C^{-n}$. *Kc* is given by the intersection with the y axis and *n* is given by the slope. *Kc* and *n* are weekly depending on material properties.

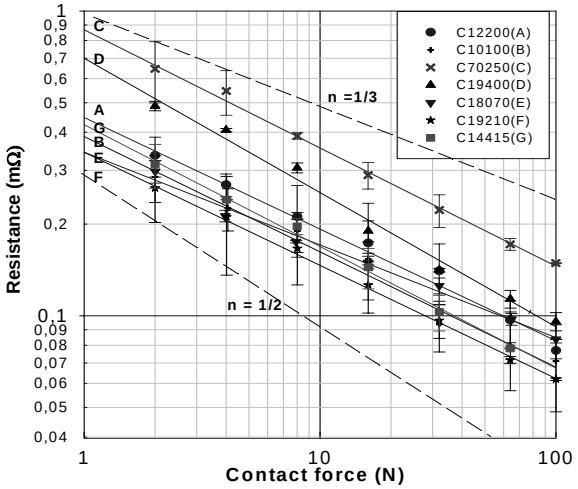

Fig. 8 Experimental contact resistance for different materials in indentation test (solid curves are $R_C = K_{ce} F_C^{-n}$) (Double logarithmic scale)

The power *n* and K_{ce} (indexed e for experimental) are listed in the Table 2 and plotted in bar chart in Fig. 9.

(C) copper alloy presents a low conductivity, high hardness and Young modulus; it has the highest K_c value and subsequent contact resistance.

Table 2 Constant values of resistance law in indentation case

	Experimental		Holm n=0.3	Analytical Sridhar		Numerical	
Mat	K_{ce} m ΩN^n	*n*	K_{cH} m ΩN^n	K_{cS} mΩN^n	*n*	K_{cn} m ΩN^n	*n*
A	0.44	0.36	0.31	0.35	0.45	0.30	0.39
B	0.38	0.37	0.24	0.27	0.45	0.23	0.39
C	0.86	0.38	0.59	0.66	0.37	0.53	0.32
D	0.69	0.44	0.37	0.39	0.37	0.33	0.32
E	0.34	0.30	0.32	0.36	0.38	0.30	0.33
F	0.34	0.37	0.25	0.28	0.39	0.23	0.33
G	0.42	0.39	0.28	0.31	0.40	0.26	0.33

However, the exponent *n* values are distributed around 1/3 which is given by elastic Hertz model. Similar power law can be find by using Holm [12] formula $Rc=\rho/2a$ and Hertz elastic contact radius area $a = \left(\frac{3F_C R}{4E^*}\right)^{1/3}$ (3)

where E* is given by : $\frac{1}{E^*} = 2.\frac{(1-\gamma^2)}{E}$ (4)

γ is the Poisson's coefficient (equal to 0.33) and E the Young's modulus.

In fact, by combining these two formulas one obtains:

$$R_{cH} = 9/20 R^{-1/3} \rho E^{1/3} F_c^{-1/3} = K_{cH} F_c^{-1/3} \quad (5)$$

Using the material properties (Table 1), one has calculated $K_{cH} = 9/20 R^{-1/3} \rho E^{1/3}$ which was already listed in the Table 2. These constant values K_{cH} (Holm's formula) are quite lower than the experimental values K_{ce}. This is due to the elastic nature of this contact radius which is not valid in our high force domain.

Regarding this discrepancy and to taking into account the plastic deformation, we try to apply the elastoplastic analytical (Sridhar) model and the numerical model. In The elastoplastic model proposed by Sridhar [7] the contact radius *a* is shared into elastic part and plastic part is given by:

$$a = \left[\left(\frac{3F_C R}{4E}\right)^{q/3} + \left(\frac{F_c}{C_f \pi \sigma_y}\right)^{q/2}\right]^{1/q} \quad (6)$$

where C_f =2.76 is constant and the power *q*=5 is the blending parameter.

Using the Yield stress σ_y listed in the Table 1, one has calculated the contact resistance based to the previous radius *a* and Holm formula. The K_{cS} (Sridhar's formula) obtained by the upper elastoplastic analytical was still lower than the K_{ce} experimental values (Table 2).

Finally, using the described computation method (FEM, Ansys, ideal surfaces), we have calculated and drawn in Fig. 10 contact resistance values versus contact forces.

The fitted curves with the previous power law give the constants values K_{cn} (from numerical results) and *n* which are listed in the Table 2 and plotted in Fig. 9 and in Fig. 10.

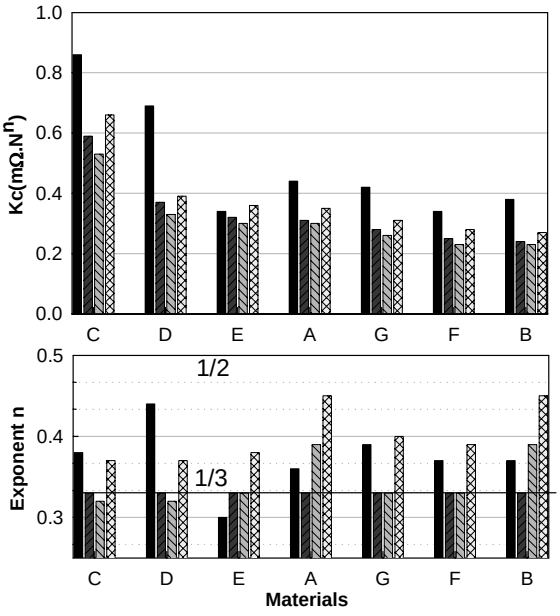

Fig. 9 Experimental and calculated constant values K_c (K_{ce}, K_{cH}, K_{cS}, K_{cn}) and *n*

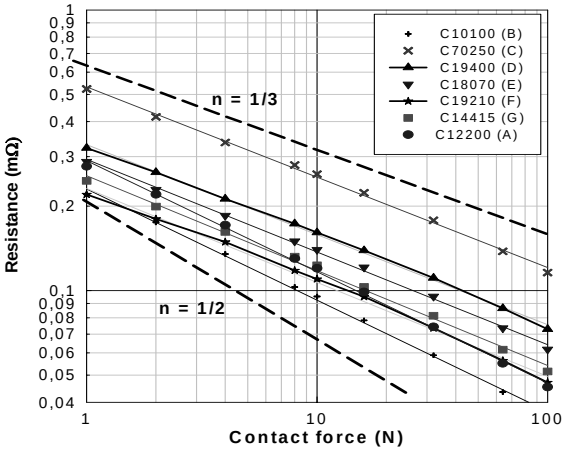

Fig. 10 Numerical resistance for different copper alloys indentation : without roughness (solid curves $R_c = K_{cn} F_c^{-n}$) (Double logarithmic scale)

We remark that *n* values are distributed between 0.3 and 0.4 for the numerical and experimental contact resistance (Table 2). But numerical K_{cn} and K_{CS} issued from this two elastoplastic model are still lower than the experimental K_{ce}. This difference between the numerical and experimental values can be explained by the contact surface roughness and asperities. As it was mentioned in the literature [14], this phenomenon is well known as the contact spots conduction mechanism located in the contact area.

In other more elaborate theory based on contact spots number *m* with radius *b*, further term $\rho / 2mb$ is added to Holm equation $\rho / 2a$. This additional contribution may increase the calculated value of contact resistance and should better convergence between K_{ce} and K_{cn} but *b* and *m* characteristics remain unknown.

Therefore, by introducing the roughness of the contact surface in numerical modelling we have attempt to reach and correct numerical values and tend to experimental resistance values. For more clarity of the graph only one material (A) was plotted and contact resistance results was shown in (Fig. 11).

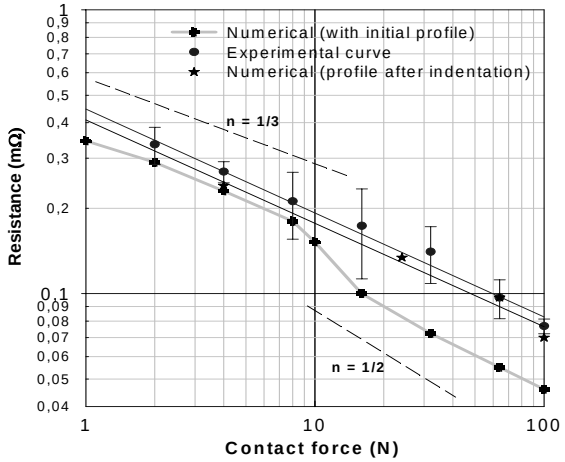

Fig. 11 Contact resistance for indentation test for A alloy (Double logarithmic scale)

The main result is a transition of resistance data around 10N of force value. For the forces values less than 10 N, the numerical values of *Rc* are higher than for those obtained by previous calculation without roughness (Fig. 10) but it's tend to the experimental resistance values. However, when the load exceeds 16 N the roughness contribution seems to be minor and the results tends to the previous resistance value calculated with ideal surface (Fig. 10). For this material at 16N, the high pressure in the contact zone (420 MPa) induces asperity crushing phenomena so their effect on electrical area is stomped. Unfortunately, for higher forces a remained discrepancy between experimental and numerical data is still observed.

To improve the convergence of the numerical model to the experimental data some contact spot resulted by indentation should be taken into account. In fact as it shown in Fig. 12 the resulted contact surface topography confirm that contact area includes some spots caused by high forces indentation.

Finally substituting the initial profile by the resulted profile after indentation (Fig. 12) the numerical modelling data approaches the experimental value (Fig. 11- value with a label).

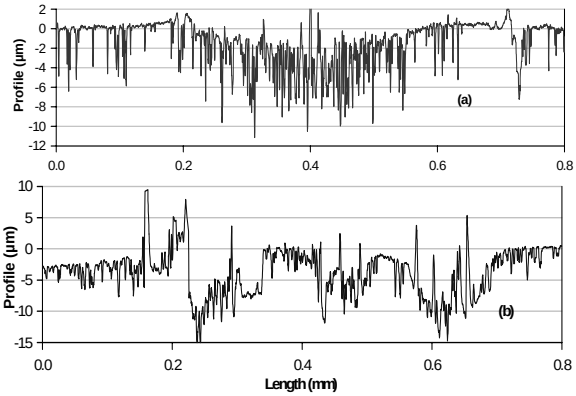

Fig. 12 Plane part profiles (a) after indentation test and (b) after insertion phase

B. Insertion test

The resistance value at the end of insertion is a main criterion for connector. This second test described in Fig 2b is made to simulate such contact mechanism. Fig. 13 shows similar decrease of contact resistance versus forces to indentation.

As in the indentation case contact resistance is well fitted to a similar law $R_c = K_c F_c^{-n}$. As expected the insertion test gives lower resistance values than that obtained in the case of the indentation test (Fig. 8). Obviously this is due to contact surfaces smoothing and subsequent area increasing during insertion. In fact, calculation sustains that contact area at 100 N is majored approximately by 20 % compared to the case of insertion test.